AIAA JOURNAL
Vol. 39, No. 10, October 2001

Design of Modal Transducers by Optimizing Spatial Distribution of Discrete Gain Weights

Jichul Kim,* Joon-Seok Hwang,† and Seung Jo Kim‡
Seoul National University, Seoul 151-742, Republic of Korea

A general method is developed of designing distributed modal transducers, especially for use in the active vibration control of structure. For this purpose, a new two-dimensional modal transducer theory has been developed. This theory is based on the finite element model of the structure, which makes it possible to determine spatial gain distribution of the specific modal transducer without restrictions on the geometry and boundary conditions of the structure. Although the optimal gain distribution can be obtained theoretically, there is no practical means of implementing it. Therefore, two design methods of distributed modal transducer are developed, which optimize available parameters of piezoelectric film to approximate optimal gain distribution best. The first method uses multilayered polyvinylidene fluoride (PVDF) films as a single transducer. The electrode pattern, the lamination angle, and the relative poling direction of each PVDF layer are optimized to obtain the desired transducer. In the second method, the whole electrode area on a single PVDF film is divided into several segments, and the gain weight imposed on each segment by interface circuit is optimized. Sensor/actuator systems for the vibration control of cantilever composite plate are designed using the proposed methods. The performance of the designed transducers is verified experimentally. The real-time vibration control of integrated smart structure has been successfully achieved.

Nomenclature

$\boldsymbol{B}_{k_s}$	=	induced charge interpolation matrix for the k_sth sensor layer
$\boldsymbol{B}_s$	=	induced charge interpolation matrix
$\boldsymbol{D}$	=	nonnegative-definite solution to the algebraic Riccati equation
$\boldsymbol{e}_i$	=	basis for the null space of $\Phi_R^T \boldsymbol{B}_s$
e_{ij}	=	piezoelectric stress constant
$\boldsymbol{G}$	=	gain-weight vector
h_i	=	modal observability measure for the ith mode
J_a	=	performance index for the actuator
J_s	=	performance index for the sensor
$\boldsymbol{K}$	=	global stiffness matrix
$\boldsymbol{M}$	=	global mass matrix
m	=	nullity of $\Phi_R^T \boldsymbol{B}_s$
$P(x, y)$	=	spatial gain distribution within a piezoelectic layer
$\boldsymbol{P}_{k_s}$	=	spatial gain vector of k_sth piezoelectric lamina
q	=	induced charge
R	=	weighting on the control signal
S	=	effective surface electrode domain
$\boldsymbol{T}$	=	electrode partition matrix
$\boldsymbol{U}$	=	nodal degree of freedom vector
u_j	=	nodal degree of freedom
v_a	=	control voltage applied to actuator
v_{ka}	=	control voltage applied to kth actuator layer
w	=	transverse displacement
z_{k_s}	=	distance from neutral plane to midplane of the k_sth sensor layer
α_i, β_i	=	coefficient of linear combination
η_i	=	ith modal coordinate
Φ_R	=	modal matrix
ϕ_i	=	ith eigenvector
$\psi_j(x, y)$	=	Hermite interpolation function
$\Omega^{(j)}$	=	integration domain of jth finite element

Received 24 October 2000; revision received 10 March 2001; accepted for publication 11 March 2001.

*Graduate Student, Department of Aerospace Engineering; currently Researcher, Third R&D Center (2-7 Division), Agency for Defense Development, Daejon 305-600, Republic of Korea.

†Ph.D Candidate, Department of Aerospace Engineering.

‡Professor, Department of Aerospace Engineering; sjkim@snu.ac.kr. Member AIAA.

Introduction

IN the vibration control of a continuum structure, the presence of uncontrolled or unmodeled modes within the bandwidth of the closed-loop system results in the well-known phenomenon of spillover.[1] The adverse effect of spillover can be prevented by special control schemes.[2] However, the elimination of spillover must be considered in view of sensor/actuator design to apply various modern control strategy on the vibration control of the structure. For this purpose, the concept of modal transducer[3] can be effectively used. For the implementation of modal transducer, distributed piezoelectric transducers have relative advantage over discrete point transducers. In case of using discrete transducers, a large amount of signal processing is required in the controller, which may destabilize the control system. However, in case of using distributed piezoelectric transducers, signal processing is performed by the charge collecting phenomenon of the surface electrode of piezoelectric materials. Also, because of the ease of electrode pattern shaping, flexibility, and light weight, some work has been centered on the design of the distributed modal transducer using polyvinylidene fluoride (PVDF) film.

Lee[4] generalized the classical laminated plate theory, including the effect of laminated piezoelectric layers, and established the concept of distributed modal transducer using PVDF film. Burke and Hubbard[5] studied the effect of spatial gain distribution of distributed transducer on the vibration control of two-dimensional structure. Miller et al.[6] developed an algorithm to determine the specific piezoelectric field distributions required to implement modal transducers in anisotropic rectangular plates. Tzou et al.[7] proposed spatially distributed orthogonal piezoelectric actuators that are orthogonal to undesirable modes. Although their theory was based on shell structure, no practical implementation method was suggested, and one-dimensional circular ring shell was used as a case study. Sullivan et al.[8] implemented spatial gain distribution in plate sturcture by optimizing triangular-shaped transducers and their gain weights. Because an analytical approach was used to determine shapes and gain weights of transducers, the spatial shape of transducer was confined to a triangular shape and, a plate with a simple shape and boundary condition (rectangular, simply supported) was used as a design example. There has been much work on implementing a modal transducer in one-dimensional structures such as

beam, ring, and narrow plates because required spatial gain distribution can be easily realized by varying the width of the distributed transducer. However, nobody has suggested a practical method for implementing the required spatial gain distribution in general, arbitrary two-dimensional structures.

The objective of the present work is to develop a systematic procedure for design and implementation of a distributed modal transducer in a two-dimensional structure. A new two-dimensional modal transducer theory based on the finite element method will be introduced to obtain the optimal gain distribution required for a specific modal transducer. For practical implementation, two design methods of a distributed modal transducer, which optimize spatial distribution of available discrete gain values to approximate optimal gain distribution best, will be presented. Last, validity of the whole design procedure will be checked through a real-time vibration control experiment.

Finite Element Modeling

A two-dimensional plate structure integrated with piezoelectric sensor and actuator layers is modeled using the finite element method. The sum of induced charge from the sensor layers under the bending of the structure is described by the following sensor equation[4]:

$$q(t) = -\sum_{k_s} z_{k_s} \int_S \left[e_{31} \frac{\partial^2 w}{\partial x^2} + e_{32} \frac{\partial^2 w}{\partial y^2} + 2e_{36} \frac{\partial^2 w}{\partial x \partial y} \right]_{k_s} \times P_{k_s}(x, y)\, dx\, dy \tag{1}$$

In the formulation of the four node plate bending elements, transverse displacement w is interpolated by the expression

$$w = \sum_{j=1}^{12} u_j \psi_j(x, y) \tag{2}$$

The spatial gain distribution of a piezoelectric layer is modeled to have a constant value $p_{k_s}^{(e)}$ within an element. However each element has a different gain value. Substitution of Eq. (2) for w in Eq. (1) gives the following finite element model of the sensor equation:

$$q(t) = \sum_{k_s} \boldsymbol{P}_{k_s}^T \boldsymbol{B}_{k_s}^T \boldsymbol{U} \tag{3}$$

where $\boldsymbol{P}_{k_s}$ is the vector whose ith element represents the gain on the charge induced from the ith finite element in k_sth piezoelectric lamina and $\boldsymbol{B}_{k_s}$ is the matrix defined as

$$\left(\boldsymbol{B}_{k_s}\right)_{ij} = -\int_{\Omega^{(j)}} z_{k_s} \left(e_{31} \frac{\partial^2 \psi_i}{\partial x^2} + e_{32} \frac{\partial^2 \psi_i}{\partial y^2} + 2e_{36} \frac{\partial^2 \psi_i}{\partial x \partial y} \right)_{k_s} dx\, dy \tag{4}$$

where $\Omega^{(j)}$ is the integration domain of jth finite element.

The actuator equation, which discribes the dynamic behavior of the integrated structure under the influence of the piezoelectric actuator layer, can be also discretized using the same finite element formulation as follows:

$$\boldsymbol{M}\ddot{\boldsymbol{U}} + \boldsymbol{K}\boldsymbol{U} = \sum_{k_a} \boldsymbol{B}_{k_a} \boldsymbol{P}_{k_a} v_{k_a} \tag{5}$$

From the reciprocal relationship between piezoelectric sensors and actuators,[4] the actuator influence matrix

$$\sum_{k_a} \boldsymbol{B}_{k_a} \boldsymbol{P}_{k_a}$$

of Eq. (5) and sensor matrix

$$\sum_{k_s} \boldsymbol{P}_{k_s}^T \boldsymbol{B}_{k_s}^T$$

of Eq. (3) are the transposed forms of each other.

Two-Dimensional Modal Transducer Theory

For the two-dimensional structure with simple geometry and boundary conditions, the spatial gain distribution required for the specific modal transducer can be determined by inspecting the analytic solution of its eigenstructure.[4] However, if the geometry and boundary conditions of the structure are complicated, there is no general method for determining the spatial gain distribution. In this section, we develop a new two-dimensional modal transducer theory to overcome this limitation.

When the single piezoelectric layer is used for the design of a modal transducer, Eq. (3) becomes

$$q(t) = \boldsymbol{P}_s^T \boldsymbol{B}_s^T \boldsymbol{U} \tag{6}$$

In the development of the vibration control strategy, it is generally impractical to consider all modeled modes. Therefore, through modal decomposition, the modal reduction can be achieved by considering only lowest N_r modes among the total N modes:

$$\boldsymbol{U} = \sum_{i=1}^{N} \phi_i \eta_i(t) \approx \sum_{i=1}^{N_r} \phi_i \eta_i(t) \tag{7}$$

When Eq. (7) is substituted into Eq. (6),

$$q(t) = \sum_{i=1}^{N_r} \boldsymbol{P}_s^T \boldsymbol{B}_s^T \phi_i \eta_i(t) \tag{8}$$

From Eq. (8), it is clear that for the piezoelectric transducer to sense only the jth modal coordinate, its spatial gain distribution vector $\boldsymbol{P}_s$ must satisfy the following condition:

$$(\boldsymbol{B}_s \boldsymbol{P}_s, \phi_i) = C \delta_{ij} \qquad (i = 1, \ldots, N_r) \tag{9}$$

where $(\cdot, \cdot)$ denotes the inner product of two vectors and C is a constant. This condition states that vector $\boldsymbol{B}_s \boldsymbol{P}_s$ must be orthogonal to all ϕ_i except ϕ_j. Among the vectors $\boldsymbol{P}_s$ satisfying condition (9), we must find an optimal $\boldsymbol{P}_s$ that is most appropriate for the observation of the jth mode. The modal observability measure[9] for the jth mode,

$$h_j = \frac{\left| \boldsymbol{P}_s^T \boldsymbol{B}_s^T \phi_j \right|}{\| \boldsymbol{B}_s \boldsymbol{P}_s \| \, \| \phi_j \|} \tag{10}$$

is used as the appropriateness measure. Therefore, finding optimal gain distribution $\boldsymbol{P}_s$ to create a modal transducer for the jth mode can be represented in the constrained optimization problem of the following form:

$$\begin{aligned} &\text{maximize} && [h_j(\boldsymbol{P}_s)]^2 \\ &\text{subject to} && (\boldsymbol{B}_s \boldsymbol{P}_s, \phi_i) = 0 \qquad (i = 1, \ldots, N_r. \quad i \neq j) \end{aligned} \tag{11}$$

For ease of the following derivation, Eq. (11) is represented in the following matrix form:

$$\begin{aligned} &\text{maximize} && \frac{\boldsymbol{P}_s^T \boldsymbol{B}_s^T \phi_j \phi_j^T \boldsymbol{B}_s \boldsymbol{P}_s}{\| \boldsymbol{B}_s \boldsymbol{P}_s \|^2 \| \phi_j \|^2} \\ &\text{subject to} && \Phi_R^T \boldsymbol{B}_s \boldsymbol{P}_s = 0 \end{aligned} \tag{12}$$

where Φ_R is the modal matrix, which consists of eigenvectors excluding the jth eigenvector. The constraint equation in Eq. (12) can be eliminated by expressing the polarization profile $\boldsymbol{P}_s$ as the linear combination for the basis for the nullspace of $\Phi_R^T \boldsymbol{B}_s$,

$$\boldsymbol{P}_s = \sum_{i=1}^{m} \boldsymbol{e}_i \alpha_i \equiv \boldsymbol{E}\alpha \tag{13}$$

When Eq. (13) is substituted into Eq. (12), the constrained optimization problem Eq. (12) can be expressed as an unconstrained optimization problem of the following form:

$$\text{maximize} \quad \frac{\alpha^T \left(\boldsymbol{E}^T \boldsymbol{B}_s^T \phi_j \phi_j^T \boldsymbol{B}_s \boldsymbol{E} \right) \alpha}{\alpha^T \left(\| \phi_j \|^2 \boldsymbol{E}^T \boldsymbol{B}_s^T \boldsymbol{B}_s \boldsymbol{E} \right) \alpha} \tag{14}$$

From Rayleigh's inequality (see Ref. 10), the solution of the optimization problem Eq. (14) is the eigenvector $\alpha_{\max}$ corresponding to the maximum eigenvalue of the following eigenvalue problem:

$$\left(\boldsymbol{E}^T\boldsymbol{B}_s^T\phi_j\phi_j^T\boldsymbol{B}_s\boldsymbol{E}\right)\alpha = \lambda\left(\|\phi_j\|^2\boldsymbol{E}^T\boldsymbol{B}_s^T\boldsymbol{B}_s\boldsymbol{E}\right)\alpha \tag{15}$$

Therefore, optimal spatial gain distribution $\boldsymbol{P}_{\text{opt}}^{(j)}$ for the modal transducer for the jth mode is

$$\boldsymbol{P}_{\text{opt}}^{(j)} = \boldsymbol{E}\alpha_{\max} \tag{16}$$

The multimode modal transducer can also be obtained by linear combination of modal transducers for each target mode,

$$\boldsymbol{P}_{\text{opt}} = \sum_{j\,=\,\text{target modes}} \boldsymbol{P}_{\text{opt}}^{(j)}\beta_j \tag{17}$$

As an example, the optimal gain distribution required to realize the modal transducer for the first mode of a graphite/epoxy composite plate is obtained using the proposed method. The plate in this example is clamped at one side and free at the others and has a stacking sequence of $[\pm 45\ \text{deg}]_S$. The size of the plate is 150 mm in length and 100 mm in width, and each ply of the laminate has a nominal thickness of 0.125 mm. Figure 1 shows a schematic view of the integrated structure. The lamination angle of the PVDF film is fixed to zero. In the modal reduction, the lowest five modes are considered, that is, $N_r = 5$ in Eq. (7). Obtained optimal gain distribution is shown in Fig. 2. Measures of observability for this transducer are shown in Table 1. We note that residual modes are completely unobservable using this transducer.

Table 1 Measures of observability

Mode	Observability measure
1	0.1608
2	0
3	0
4	0
5	0

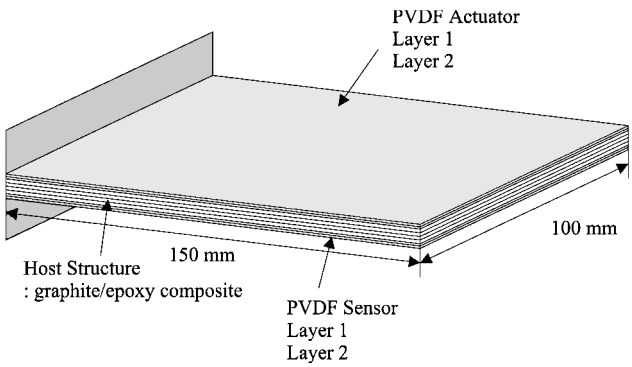

Fig. 1 Schematic view of the integrated structure.

Design of Modal Transducer Using Multilayered PVDF Films

For the experimental realization of the prescribed spatial gain distribution, some research[5] suggested the method of changing original poling intensity of the PVDF film using PZT powder or through the repoling process. However, these procedures are impractical. In this section, we approximate the desired gain distribution by optimizing electrode patterns, lamination angles, and relative poling directions of multilayered PVDF layers as a practical means for implementing spatial gain distribution.

In case of a single PVDF film, the gain is 1 in the surface area with an effective electrode and 0 in the area without an effective electrode. Therefore, optimization of the electrode pattern equals the approximation of the optimal gain distribution using discrete gain values $\{1, 0\}$. In the case of multilayered PVDF films, not only the electrode pattern and lamination angle but also the poling direction of each layer is an important design parameter. For example, if the relative poling directions of two layers of PVDF films with the same electrode patterns and lamination angles are opposite, then the electric charge induced from each layer almost cancels out each other. However, the total induced charge is twice the amount of the electric charge induced from each layer if the relative poling directions are the same. Therefore, optimization of each layer's electrode pattern corresponds to the approximation of the optimal gain distribution using discrete gain values $\{2, 1, 0\}$ in the case of same poling directions and $\{1, 0, -1\}$ in the case of opposite poling directions, respectively.

Sensor Design Criterion

Because the design of a modal transducer by optimizing the electrode pattern is an approximation process, we cannot make the residual modes completely unobservable. Instead, sensor design is based on the criterion of minimizing observation spillover from residual modes. Electric charges induced from residual modes are minimized, whereas those from the control modes are maximized. This procedure can be represented as the following optimization problem:

$$\text{maximize} \quad J_s \equiv \frac{\min(h_i)}{\max(h_j)} \begin{cases} i = \text{control modes} \\ j = \text{residual modes} \end{cases} \tag{18}$$

where h_i is defined as

$$h_i = \frac{\left|\sum_{k_s} \boldsymbol{P}_{k_s}^T\boldsymbol{B}_{k_s}^T\phi_i\right|}{\left\|\sum_{k_s} \boldsymbol{B}_{k_s}\boldsymbol{P}_{k_s}\right\|\,\|\phi_i\|} \tag{19}$$

$\boldsymbol{P}_{k_s}$ is the vector representing the electrode pattern of the k_sth layer:

$$\boldsymbol{P}_{k_s}(i) = \begin{cases} 1 & \text{if the electrode on } i\text{th element is on} \\ 0 & \text{if the electrode on } i\text{th element is off} \end{cases} \tag{20}$$

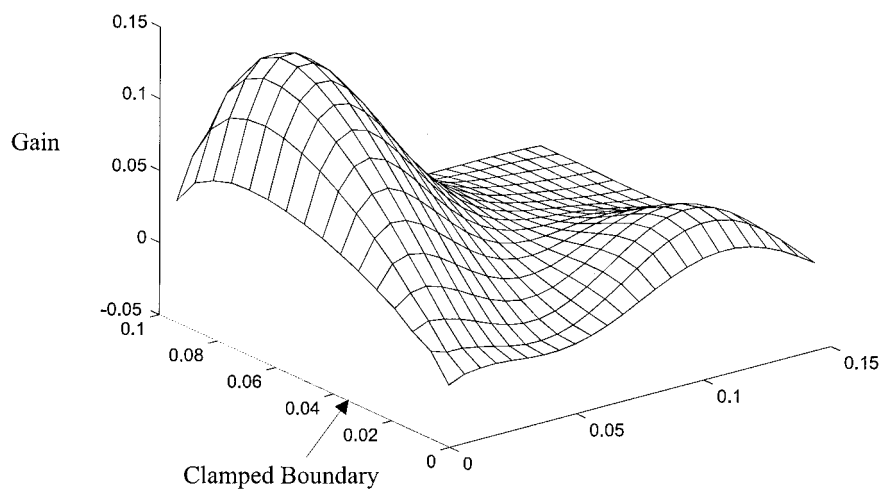

Fig. 2 Optimal gain distribution for mode 1 transducer (0 deg).

By optimizing on or off of the electrode on each element, we can best approximate the modal sensor that acts as a modal bandpass filter in the spatial domain that passes only the specific modes.

Actuator Design Criterion

In the process of actuator design, only the control modes are considered because the instability caused by the observation of residual modes is minimized by the accompanying modal sensor. The actuator is designed to minimize the system energy in the control modes, which is represented as a quadratic cost functional given by

$$J = \frac{1}{2}\int_0^\infty \left[z^T \boldsymbol{Q} z + R v_a^2\right] \mathrm{d}t \tag{21}$$

where $z = [\eta_c \quad \dot{\eta}_c]^T$ is the state of the total system and

$$\boldsymbol{Q} = \begin{bmatrix} \Lambda_c & 0 \\ 0 & \boldsymbol{I} \end{bmatrix} \tag{22}$$

The minimum cost $J_{\min}$ is given by

$$J_{\min} = z^T(t_0)\,\boldsymbol{D} z(t_0) \tag{23}$$

where $\boldsymbol{D}$ is the unique nonnegative-definite solution to the algebraic Riccati equation.[11] In Eq. (23), $J_{\min}$ depends on the initial states $z(t_0)$. Therefore, the actuator is designed to minimize $J_{\min}$ for the worst-case initial condition, resulting in the following optimization problem[11]:

$$\text{minimize} \quad J_a \equiv \max_{\|z_0\|=1} \left(z_0^T \boldsymbol{D} z_0\right) \tag{24}$$

From Rayleigh's inequality, the solution of the problem $\max_{\|z_0\|=1}(z_0^T \boldsymbol{D} z_0)$ is the maximum eigenvalue of the matrix $\boldsymbol{D}$. This method optimizes performance uniformly in initial conditions. The weighting on the control signal R in Eq. (21) has an influence on the magnitude of $J_{\min}$. However, it does not affect the optimized electrode pattern of the actuator.[12]

Genetic Algorithm

The genetic algorithm[13] is used for the optimization of each PVDF layer's electrode pattern and lamination angle. The optimization of the electrode pattern, which determines whether an electrode segment is on or off, is in itself a discrete problem. Thus, it can be easily dealt with using the genetic algorithm. However, the optimization of lamination angle is not a discrete problem but a continuous one. Therefore, continuous lamination angles between -90 and $+90$ deg are encoded into discrete values using binary 5-bit string. There are 36 discrete values if the lamination angle is divided at intervals of 5 deg. However, a binary 5-bit string can represent only 32 $(= 2^5)$ discrete values. Therefore, the lamination angle between -70 and $+70$ deg is divided at intervals of 5 deg and the remainder at intervals of 10 deg, thus resulting in a total of 32 discrete values.

Design Results

For the real-time vibration control of the integrated structure shown in Fig. 1, a modal sensor and an actuator for the first and second modes are designed using two layers of PVDF films each. According to the finite element analysis, the natural frequencies for the lowest five modes are 12.9, 60.6, 78.9, 179.2, and 208.8 Hz. To avoid spillover from the residual modes, signals from the residual modes must be filtered out. However, because the second and third natural frequencies are closely located, it is difficult to minimize the signal from third mode without phase lag using a time-domain filter.[14] In this case, a distributed piezoelectric modal sensor and actuator, a kind of modal bandpass filter in the spatial domain, can be applied effectively.

The sensor and actuator have been designed for the cases of two-layered PVDF films with same poling directions [sensor positive–positive (SPP) and actuator positive–positive (APP)] and two-layered PVDF films with opposite poling directions [sensor positive–negative (SPN) and actuator positive–negative (APN)]. The performances of the optimized sensors are compared with that of the sensor that is designed by simply layering the optimized result of single-layer case twice (SP2). Because each layer consists of 96 (12×8) electrode segments and its lamination angle is encoded using binary 5-bit string, the configuration of each layer is represented by a binary string of length 101:

$$\overbrace{[11010\cdots01010}^{\text{electrode pattern (96)}}\overbrace{11010}^{\text{angle (5)}}] \tag{25}$$

Modal observability measures, optimized lamination angles of the two-layered PVDF sensors, and performance indices are listed in Table 2. Figure 3 is the optimized electrode patterns of each layer of SPP, where the black region is the active electrode. The left-hand side is the clamped edge. From Table 2, distinctions in the modal observability measures are observed between control modes and residual modes. SPP shows better performance than SPN. We

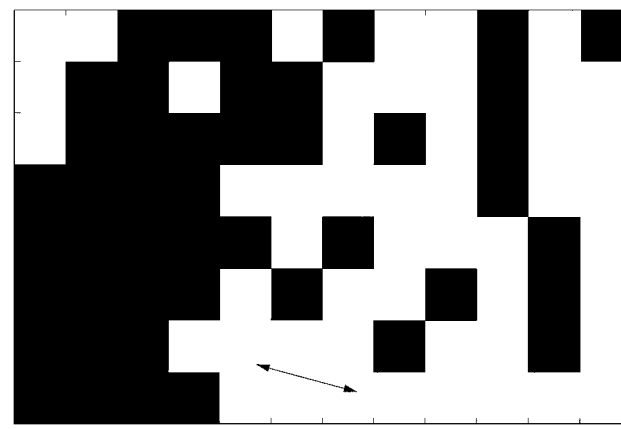

a) Layer 1 (– 15 deg)

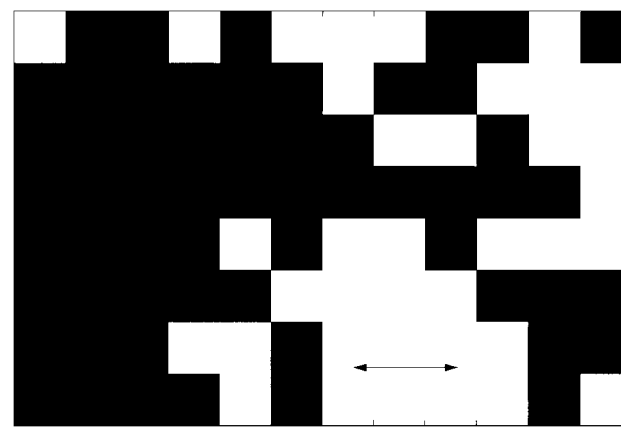

b) Layer 2 (0 deg)

Fig. 3 Optimized electrode patterns of SPP.

Table 2 Optimization results of two-layered PVDF sensors

Case	h_1	h_2	h_3	h_4	h_5	Layer 1, deg	Layer 2, deg	J_s
SPP	7.2278e−3	3.8602e−3	1.2754e−5	3.7007e−7	8.3248e−6	−15	0	302.66
SP2	3.5489e−3	2.5684e−3	1.6556e−4	1.1475e−5	2.0171e−4	−15	−15	12.733
SPN	2.1745e−3	9.3728e−4	1.1642e−7	3.9757e−6	6.9687e−6	35	0	134.50

Table 3 Optimization results of two-layered PVDF actuators

Case	Layer 1, deg	Layer 2, deg	J_a
APP	−20	−20	1.1421*e*4
APN	65	−20	2.3483*e*4

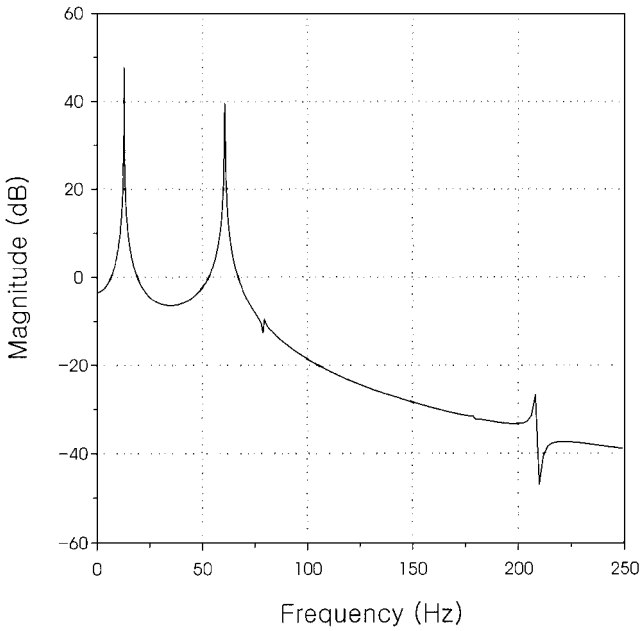

Fig. 4 FRF of SPP integrated in the structure (from numerical simulation).

can conclude that using two different positive values (SPP) is more effective than using one positive value and one negative value (SPN) in the approximation of optimal spatial gain distribution of this case. Because the performance of SPP is much better than SP2, it can be concluded that the electrode pattern and lamination angles of each layer must be optimized separately to make the most from the multilayered PVDF transducer. SPP, which shows best performance, is chosen for experiment. Figure 4 shows the numerical simulation of the frequency-response function (FRF) for the SPP integrated in the structure. Note that the signals from residual modes are almost unobservable.

Performance indices and optimized lamination angles of two-layered PVDF actuators are listed in Table 3. Figure 5 is the optimized electrode patterns of each layer of APP. Because the system energy in the control modes are much smaller than that of ANP, APP is chosen for the experiment.

Design of Modal Transducer by Optimizing Electrode Partition and Gain Weights

In this section, we will develop another method of implementing spatial gain distribution. The whole spatial area of a single PVDF film is divided into several segments, and the gain weight on each electrode segment is optimized. This concept is similar to the method developed in preceding section in the sense that they are approximations of the continuous function using discrete values. The difference between two methods is that, in the multilayer case, available discrete values are fixed to certain values based on the number of PVDF layers used and their relative poling directions. On the other hand, the method used in this section does not have such constraints on gain values. Rather, they are optimized to best approximate the continuous function.

Optimization Procedure

Sensor and actuator design criteria used in this section are the same as the multilayer case. However, in this case, spatial gain distribution vector $\boldsymbol{P}$ is determined by partitioning the whole electrode area and the gain weight on each electrode segment:

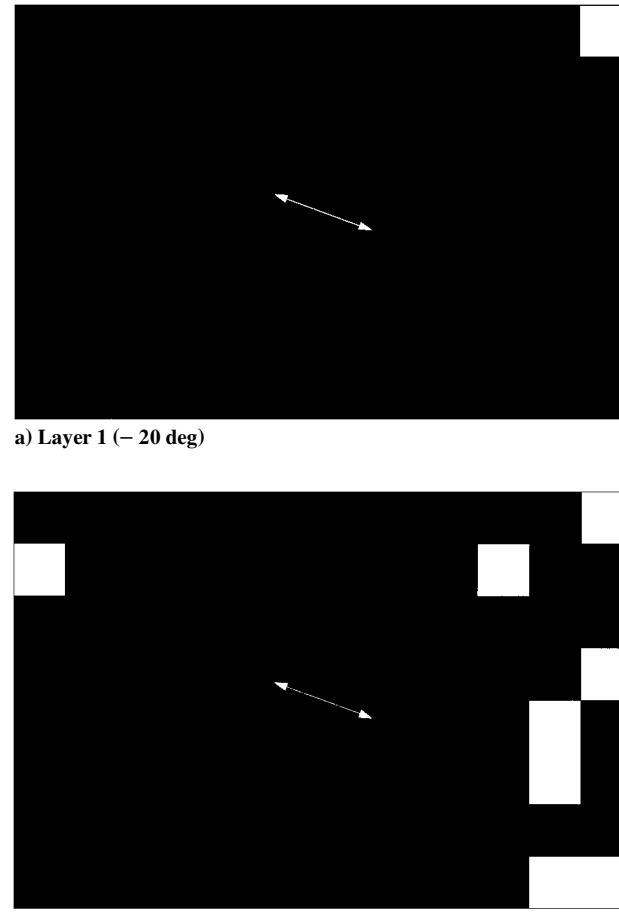

a) Layer 1 (− 20 deg)

b) Layer 2 (− 20 deg)

Fig. 5 Optimized electrode patterns of APP.

$$\boldsymbol{P} = \boldsymbol{TG} \tag{26}$$

where $\boldsymbol{T}$ is the matrix representing the electrode partition defined as

$$\boldsymbol{T}_{ij} = \begin{cases} 1 & \text{if electrode on } i\text{th element belongs to the } j\text{th segment} \\ 0 & \text{otherwise} \end{cases} \tag{27}$$

and $\boldsymbol{G}_j$ is the gain weight on the jth segment. By optimizing $\boldsymbol{T}$ and $\boldsymbol{G}$, namely, electrode partition and gain weights, we can obtain the best spatial gain distribution $\boldsymbol{P}$ that optimizes the performance index in Eq. (18) or Eq. (24).

The genetic algorithm is used for the optimization of electrode partition because dividing the whole PVDF film area into several segments [i.e., deciding each element of $\boldsymbol{T}$ in Eq. (27) to be 1 or 0] is a combinatorial optimization problem. During the genetic algorithm loop, optimization of gain weights is performed for each electrode partition using simplex search method just before the evaluation of performance index.

In the manufacturing process of the specimen, the electrode patches that belong to same segment must be connected electrically, whereas the electrode patches which belong to different segments must be separated. To provide electric isolation between different electrode segments, narrow regions of electrode between different electrode segments are automatically removed before the performance index evaluation process of the genetic algorithm. For this purpose, one electrode patch is modeled using nine FEs with different sizes. This is shown in Fig. 6. Electrode patches on the boundaries of the plate will be removed to provide enough space for the connection of the electrodes in the same segment.

Table 4 Optimization results of sensors

Parameter	S(−45 deg)	S(−30 deg)	S(−15 deg)	S(0 deg)	S(15 deg)	S(30 deg)
h_1	9.7587e−5	2.1038e−4	3.0713e−4	1.3537e−2	2.0634e−4	4.9556e−5
h_2	1.6849e−4	2.3742e−4	2.5368e−4	7.1193e−3	1.1890e−4	4.9976e−5
h_3	1.9616e−7	8.7028e−8	1.0901e−8	6.3883e−6	1.7364e−7	2.3146e−7
h_4	2.9210e−8	4.2460e−9	2.7203e−7	6.2700e−6	3.0948e−8	8.0171e−8
h_5	2.8207e−7	3.6287e−8	1.5824e−7	1.4137e−5	1.6266e−7	1.1549e−7
G_1	0	0	0	0	0	0
G_2	0.9439	0.4755	0.2784	0.9578	0.3260	0.8384
G_3	−0.3304	0.8797	−0.9605	−0.2873	−0.9454	−0.5450
J_s	345.96	2417.40	932.53	503.59	684.77	214.10

Table 5 Optimization results of actuators

Parameter	A(−60 deg)	A(−45 deg)	A(−30 deg)	A(−15 deg)	A(0 deg)	A(15 deg)	A(30 deg)
G_1	0	0	0	0	0	0	0
G_2	0.9970	0.2425	0.9942	0.9837	0.2603	0.4028	0.8158
G_3	−0.0772	−0.9701	−0.1076	−0.1797	−0.9655	−0.9153	−0.5783
J_a	25250	23842	24520	28350	36174	49861	67308

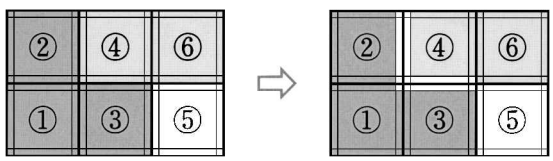

Fig. 6 Electric isolation between different segments.

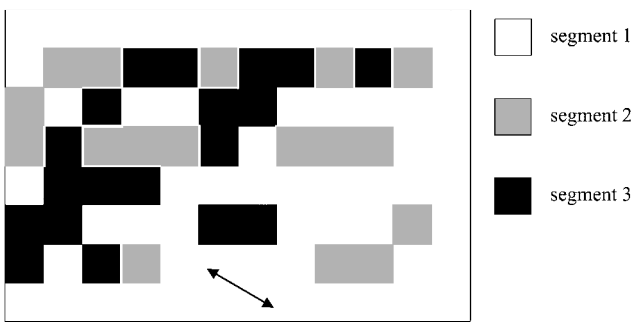

a) S(− 30 deg)

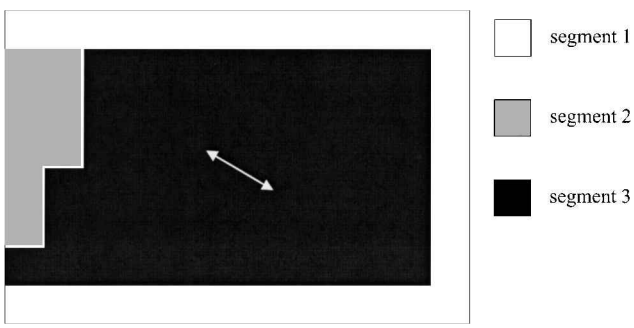

b) A(− 45 deg)

Fig. 7 Optimized electrode partitions.

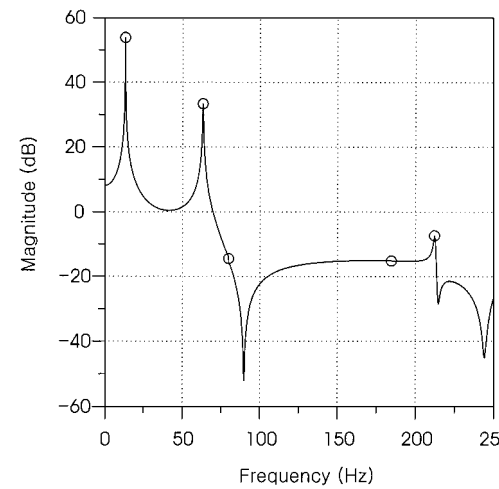

Fig. 8 FRF of S(− 30 deg) integrated in the structure (from numerical simulation).

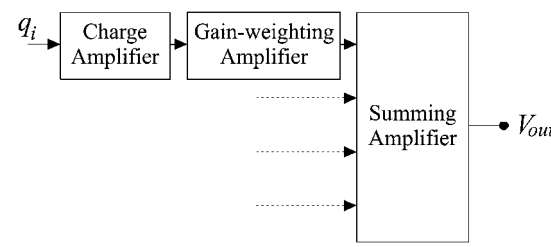

Fig. 9 Schematic diagram of the interface circuit.

Design Results

Modal sensors and actuators for the first and second modes of the structure shown in Fig. 1 are designed using the present method. Optimization is performed for the various lamination angles of the PVDF film. In the optimization procedure, the whole electrode area of a PVDF film is divided into three segments, and gain weight on the first segment is fixed to zero, that is, exclusion in the optimization because zero gain weight can be easily implemented by removing surface electrodes. Table 4 shows the performance indices, modal observability measures, and gain weights of optimized modal sensors. In Table 4, the heading S(θ) denotes the optimized sensor with lamination angle θ. Because of the anisotropic characteristic of the host structure, S(θ) and S($-\theta$) show different performances. Among the seven sensors, S(−30 deg), which shows the best performance, is chosen for experiment. Optimized electrode partition of the S(−30 deg) is shown in Fig. 7a. Figure 8 shows the numerical simulation of the frequency response for the sensor S(−30 deg) integrated in the structure. The amplitudes in the third mode to the fifth mode show dramatic reduction compared with those of the first and second modes.

For each lamination angle, an actuator has been designed to minimize the system energy in the control modes. Performance indices and optimized gain weights are listed in Table 5. The heading A(θ) indicates optimized actuator with lamination angle θ. The actuator with lamination angle −45 deg shows the minimum system energy in control modes. Thus, A(−45 deg) is chosen for experiment. Optimized electrode partition of A(−45 deg) is shown in Fig. 7b.

The optimized gain weights in Tables 4 and 5 are implemented using an interface circuit. Figure 9 shows the schematic diagram of

the interface circuit. Noninverting and inverting amplifiers are used for positive and negative gain-weighting amplifiers, respectively.[15] Required gain weight can be obtained by adjusting the value of the resistor in each amplifier.

Real-Time Vibration Control

Experimental Setup

Two specimens were manufactured for the experiment. For the first specimen (SPEC-I), SPP in Fig. 4 is used as sensor and APP in Fig. 5 as actuator. For the second specimen (SPEC-II), S(−30 deg) in Fig. 7a is used as sensor and A(−45 deg) in Fig. 7b as actuator. Kynar PVDF 52 μm thick film is used.

Figure 10 shows the experimental setup. The charge amplifier gain is set to 10^8 V/F. Cutoff frequencies of the low-pass filters are set to 100 Hz, which lies between the third and fourth natural frequencies of the structure. The output of the low-pass filter is passed to the personal computer, which contains A/D and D/A converter boards. The maximum voltage amplitude of the control signal is set to ±4 V. A high-voltage amplifier is used to amplify the control signal by the gain of 100 to drive the PVDF actuator. In the SPEC-II case, output from each electrode segment is individually gain weighted by the gain-weighting amplifier. Then, all of the gain weighted outputs are added together in a summing amplifier. A control signal is also given to each electrode segment with different gain weight imposed by the gain-weighting amplifier.

An impulse disturbance is employed in the experiment. The excitation force signal from the impact hammer and the sensor signal from the charge amplifier are given to the signal analyzer for use in the FRF calculation.

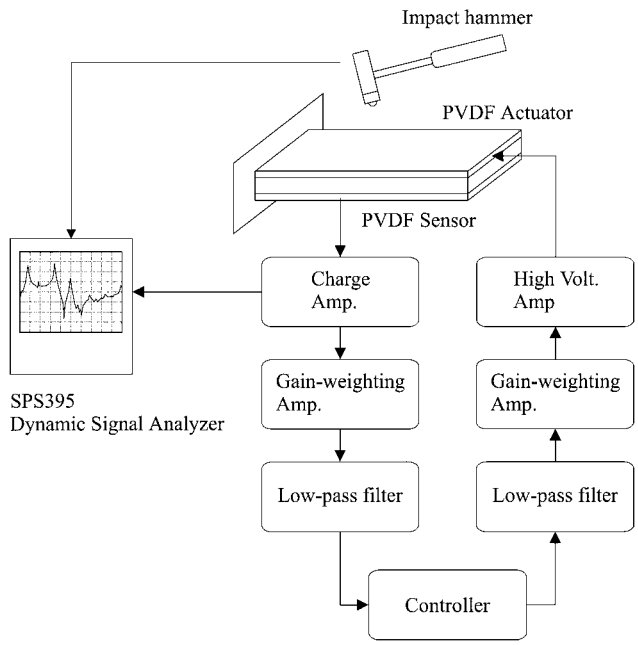

Fig. 10 Experimental setup.

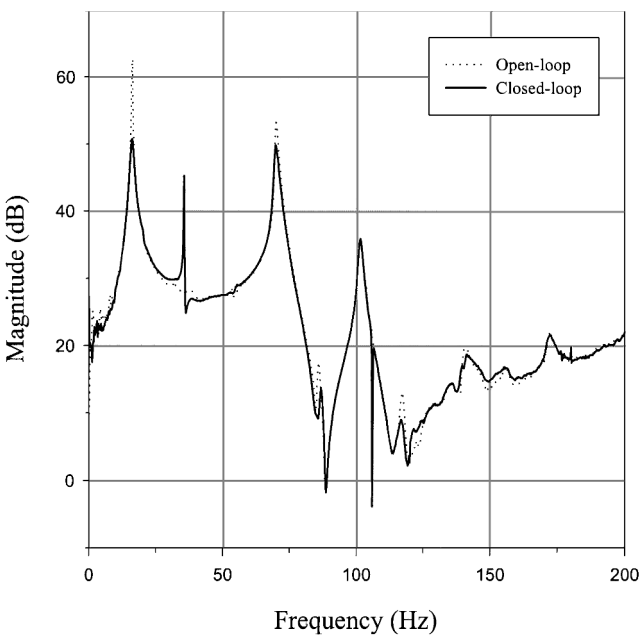

Fig. 11 FRF of SPEC-I (from experiment).

Experimental Results and Discussion

The experimentally obtained open-loop FRF between impulse input and the optimized sensor of each specimen is shown in Figs. 11 and 12. The signals from the control modes are approximately 10 times (20 dB) larger than those from the residual modes. Therefore, these sensors can be used effectively for the minimization of the observation spillover from the residual modes. Closed-loop tests were conducted to show that using a linear quadratic Gaussian (LQG) controller with the optimized sensor/actuator system would result in a stable system with the added damping. The closed-loop

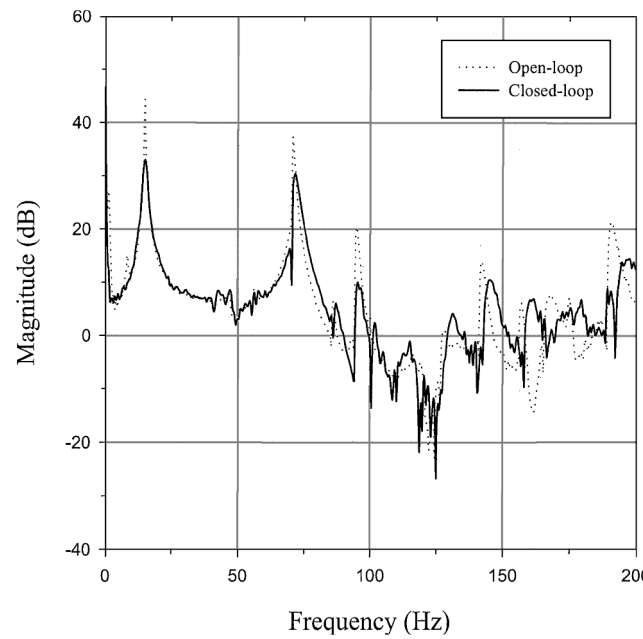

Fig. 12 FRF of SPEC-II (from experiment).

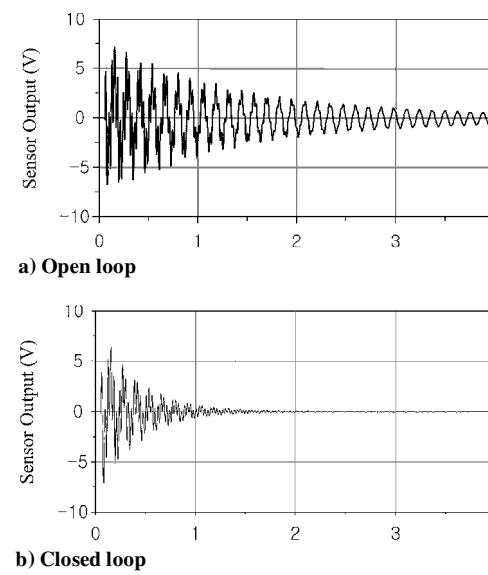

Fig. 13 Open- and closed-loop time responses of SPEC-I (from experiment).

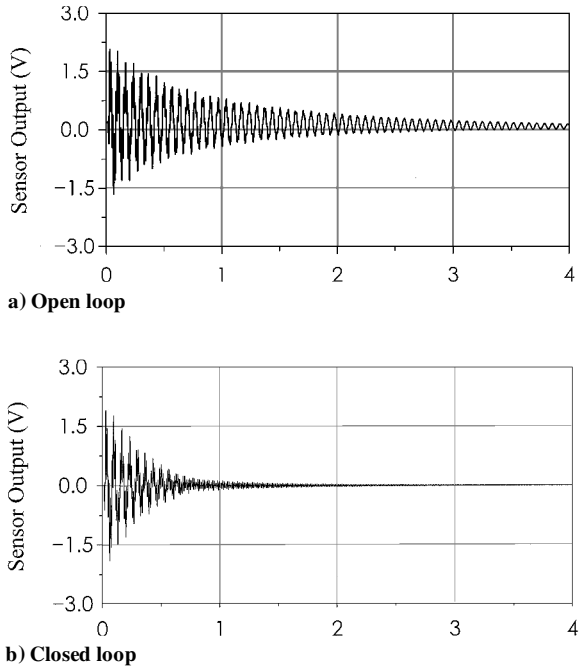

Fig. 14 Open- and closed-loop time responses of SPEC-II (from experiment).

FRFs of SPEC-I and SPEC-II are plotted in Figs. 11 and 12, respectively. These results show dramatic improvements in the damping characteristics of integrated structures. In the SPEC-I case, the modal peaks of the first and second modes are reduced 13 and 4 dB, respectively. The peak, shown around 30 Hz in the closed-loop transfer function, is not an unmodeled structural mode, but an electrical noise arising from the control equipment. In the SPEC-II case, the modal peaks of the first and second modes are reduced by 10 and 8 dB, respectively. The time responses of the SPEC-I and SPEC-II using the LQG controller as the closed-loop control law are plotted along with the open-loop responses in Figs. 13 and 14. For both specimens, settling time is reduced to approximately 25% compared with that of open-loop system.

Conclusions

Design methods developed in this paper are intended to be used for the efficient active vibration control of the exible structures. However, these design methods of modal transducer can be applied in any field where acquisition or activation of the specific vibrational mode of structure is important.

As can be seen in the experimental results, signals from the residual mode still have significant magnitude, although they are very small compared to those from the control modes. It is mainly due to the discrepancy existing between the behaviors predicted by the FE model and that exhibited by the real structure. Therefore, future effort would be also added to reduce this discrepancy for the optimal performance.

Acknowledgments

The research was supported in part by a grant from the BK-21 Program for Mechanical and Aerospace Engineering Research at Seoul National University and in part by the Ministry of Science and Technology through National Research Laboratory Programs (Contract 00-N-NL-01-C-026).

References

[1] Balas, M. J., "Feedback Control of Flexible Systems," *IEEE Transactions on Automatic Control*, Vol. AC-23, No. 4, 1978, pp. 673–679.

[2] Fanson, J. L., and Caughey, T. K., "Positive Position Feedback Control for Large Space Structures," *AIAA Journal*, Vol. 28, No. 4, 1990, pp. 717–724.

[3] Meirovitch, L., and Baruh, H., "The Implementation of Modal Filters for Control of Structures," *Journal of Guidance, Control, and Dynamics*, Vol. 8, No. 6, 1985, pp. 707–716.

[4] Lee, C. K., "Piezoelectric Laminates: Theory and Experiments for Distributed Sensors and Actuators," *Intelligent Strctural Systems*, edited by H. S. Tzou and G. L. Anderson, Kluwer Academic, Norwell, MA, 1992, pp. 75–167.

[5] Burke, S. E., and Hubbard, J. E., Jr., "Distributed Transducer Vibration Control of Thin Plates," *Journal of the Acoustical Society of America*, Vol. 90, No. 2, 1991, pp. 937–944.

[6] Miller, S. E., Oshman, Y., and Abramovich, H., "Modal Control of Piezolaminated Anisotropic Rectangular Plates Part 1: Modal Transducer Theory," *AIAA Journal*, Vol. 34, No. 9, 1996, pp. 1868–1875.

[7] Tzou, H. S., Zhong, J. P., and Hollkamp, J. J., "Spatially Distributed Orthogonal Piezoelectric Shell Actuators: Theory and Applications," *Journal of Sound and Vibration*, Vol. 177, No. 3, 1994, pp. 363–378.

[8] Sullivan, J. M., Hubbard, J. E., and Burke, S. E., "Distributed Sensor/Actuator Design for Plates: Spatial Shape and Shading as Design Parameters," *Journal of Sound and Vibration*, Vol. 203, No. 3, 1997, pp. 473–493.

[9] Hamdan, A. M. A., and Nayfeh, A. H., "Measures of Modal Controllability and Observability for First- and Second-Order Linear Systems," *Journal of Guidance, Control, and Dynamics*, Vol. 12, No. 3, 1989, pp. 421–428.

[10] Strang, G., *Linear Algebra and Its Applications*, Harcourt Brace, Fort Worth, TX, 1988.

[11] Devasia, S., Meressi, T., Paden, B., and Bayo, E., "Piezoelectric Actuator Design for Vibration Suppression: Placement and Sizing," *Journal of Guidance, Control, and Dynamics*, Vol. 16, No. 5, 1993, pp. 859–864.

[12] Ryou, J.-K., Park, K.-Y., and Kim, S.-J., "Electrode Pattern Design of Piezoelectric Sensors and Actuators Using Genetic Algorithms," *AIAA Journal*, Vol. 36, No. 2, 1998, pp. 227–233.

[13] Goldberg, D. E., *Genetic Algorithms in Search, Optimization and Machine Learning*, Addison Wesley Longman, Reading, MA, 1989, pp. 59–88.

[14] Collins, S. A., Miller, D. W., and Von Flotow, A. H., "Distributed Sensors as Spatial Filters in Active Structural Control," *Journal of Sound and Vibration*, Vol. 173, No. 4, 1994, pp. 471–501.

[15] Stout, D. F., and Kaufman, M., *Handbook of Operational Amplifier Circuit Design*, McGraw–Hill, New York, 1976, Chap. 4, pp. 1–12.

C. Pierre
Associate Editor